Amer *et al. Int J Concr Struct Mater (2023) 17:36*
https://doi.org/10.1186/s40069-023-00596-2

International Journal of Concrete Structures and Materials

RESEARCH

Open Access

Realistic Evaluation of Reinforcement Bond Strength in Alkali-Activated Slag Concrete Exposed to Elevated Temperature

Ismail Amer[1*], Mohamed Kohail[1*], M. S. El-Feky[2], Ahmed Rashad[1] and Mohamed A. Khalaf[1]

Abstract
Alkali-activated concrete (AAC) has attained great popularity since finding it as an alternative to Portland cement concrete due to its superior characteristics in terms of mechanical properties and durability, and its low negative environmental impact. This research investigated both experimentally and analytically the bond behavior between alkali-activated slag concrete (AASC) and steel rebars considering some important parameters (rebar diameter and development length-to-diameter ratio) before and after exposure to elevated temperature using beam-end bond testing technique. The obtained experimental results were compared with those obtained from applying the CEB-FIP model and the well-known available equations in the literature. A modified model was proposed for predicting the bond behavior of AASC. Results have showed that the CEB-FIP model provides more conservative values for bond strength compared to the experimentally obtained results which increases the safety level when estimating the bond strength for design purposes. The proposed modified model achieved a higher correlation with the experimental results than the CEB-FIP model at ambient temperature.

Keywords Alkali-activated concrete, GGBFS, Alkali-activation, Ambient cured, Bond behavior, Elevated temperature, Beam-end bond testing technique

1 Introduction

The environmental impact of ordinary Portland cement (OPC) production is mainly due to the energy consumed intensively in its manufacturing process. Moreover, the cement industry alone is responsible for approximately 6–7% of the total greenhouse gases emitted all over the world (Bijen, 1996; Pal, 2018; Refaat et al., 2021). To suppress these drawbacks, the construction industry is looking forward to develop innovative binders valid to be an alternative to OPC (Bastidas et al., 2008; Gong & Yang, 2000; Grutzeck et al., 2004; Khalil et al., 2020; Kotop et al., 2021; Palomo et al., 1999; Provis & Van Deventer, 2009a; Puertas et al., 2000). To that extent, the ecological dream of producing Portland cement-free concrete, started to come true, when researchers began to utilize industrial by-products or natural materials that are rich with aluminate and silicate, and activating them by alkali-activators. The obtained alkali-activated binders get mixed with both of fine and coarse aggregates and when being hardened through appropriate conditions forming alkali-activated concrete (AAC) (Amer et al., 2020, 2021a, 2021b; Davidovits, 1991; Lee & Lee, 2013; Ravikumar et al., 2010; Thomas & Peethamparan, 2015; Zhang et al., 2020). CO_2 emissions result from manufacturing alkali-activated binder is around 50–80% lower

Journal information: ISSN 1976-0485 / eISSN 2234-1315.

*Correspondence:
Ismail Amer
ismail.amer@eng.asu.edu.eg
Mohamed Kohail
m.kohail@eng.asu.edu.eg
[1] Structural Engineering Department, Faculty of Engineering, Ain Shams University, Cairo, Egypt 11517
[2] Civil Engineering Department, National Research Centre, Cairo, Egypt 12622

than OPC composites production (Duxson et al., 2007; Provis & Van Deventer, 2009b).

Many significant studies have been conducted on AAC to address the manufacturing of AAC using different types of source materials for obtaining desirable mechanical characteristics (Abdulrahman et al., 2021; Allaoui et al., 2022; Okoye et al., 2015; Xie et al., 2018), while studies concerned with its structural performance are still limited (Ma et al., 2018; Mo et al., 2016; Nikbakht et al., 2021; Unis Ahmed, et al., 2022). The bond behavior of steel-reinforced AAC is a vital property that has to be established to ensure the achievement of sufficient bond between the steel rebars and the surrounding AAC (Al-Azzawi et al., 2018; Albidah et al., 2020; Romanazzi et al., 2022; Yang, et al., 2022). Particular investigation has been performed to evaluate the bond performance between AAC and rebars (Ahmad & Bhargava, 2020; Alharbi et al., 2021a; Sarker, 2011; Sofi et al., 2007; Zhang et al., 2016). It was drawn that AAC demonstrated better bond performance compared with conventional concrete (Castel & Foster, 2015; Sarker, 2011). Also it was reported that the bond performance was improved with increasing both of the concrete cover thickness, compressive strength, and the ratio between thickness of concrete cover and diameter of rebars (Sarker, 2011). Several parameters affecting the bond performance such as compressive strength, concrete cover, rebars characteristics (mainly diameter and surface texture), confinement conditions and the bond stress–slip relationship were studied (Zhang et al., 2016). Most of studies are primarily related to investigate the bond behavior in ambient temperature. Insufficient attention has been directed towards the bond performance between AAC and rebars at high temperature (Chen et al., 2018).

Reinforcement bar bond characteristics in concrete exposed to elevated temperatures are crucial for maintaining structural integrity in case of fire. A well-established research works investigated the bond characteristics between the reinforcement bars and OPC concrete (Alharbi et al., 2021b). Some recent studies (Morley & Royles, 1980; Yin et al., 2011) revealed that the strength of concrete reduced as the temperature increased; at elevated temperature, the degradation of concrete–rebar bond strength was significant.

H.Y. Zhang et al. investigated the bond behavior of metakaolin–fly ash based AAC with different-diameter rebars, using pull-out tests, after exposure to elevated temperatures up to 700 °C. It was shown that the AAC did not demonstrate significant deterioration in bond strength except when exposed to elevated temperature above 300 °C. Also, AAC showed similar or better bond characteristics than OPC concrete with similar compressive strength (Zhang et al., 2018). Jiang et al. performed a laboratory study to investigate the steel rebar-to-paste bond behavior for both AAC and OPC concrete after exposing to very high temperatures (up to 1200 °C). This study revealed that AAC retained some residual bond strength even after exposing to 1200 °C, While OPC concrete completely disintegrated at 800 °C, which indicated to the excellent bonding performance of AAC at the extreme temperatures (Jiang et al., 2020). Ramagiri et al. reported that increasing the slag content in the blended binder (fly ash + slag) of AAC increased the bond strength of AAC at a constant activator modulus. Also, it was reported that the AAC mix that contains 30% slag in the blended binder exhibited a superior high-temperature performance in terms of residual compressive and bond strength (Ramagiri & De Maeijer, 2022). Paswan et al. investigated the bond behavior at elevated temperature up to 800 °C between rebars and fly ash–slag based AAC as a function of compressive strength, rebar diameter, embedment length and concrete cover by considering the obtained ultimate bond stress, slip, and load at failure compared with those of control cement concrete. It was concluded that the bond performance of AAC was effective compared with that of the cement concrete. Also, it was reported that the bond strength of AAC exposed to elevated temperatures increased with an increase of temperature up to 400 °C, due to the curing of low-calcium fly ash, and then decreased. The decrease in bond strength was about 69% at 800 °C (Paswan et al., 2020).

Many researches proved the superiority of AAC in the mechanical properties and durability compared with the conventional concrete. However, limited studies have been investigated the bond performance between AAC and steel rebars, and most of them were conducted using the well-known pull-out test on lollipop specimens because of its simplicity, while rare studies have used the beam-end specimens which are more realistic and accurate, because of the relative difficulty of its test setup. Moreover, researches investigating the bond behavior of AAC after exposure to elevated temperatures are still limited especially for those that used slag only as a binder. So, this paper concerned with investigating the bond behavior between AASC, using binder totally from slag, and steel rebars considering the rebar diameter and development length-to-diameter ratio using the beam-end technique, which is consider the most effective technique, at both ambient and elevated temperatures.

2 Experimental Program

2.1 Materials

GGBFS was used as the binder in this study. The chemical composition of GGBFS is presented in Table 1. The coarse aggregate was natural crushed limestone with nominal maximum size of 10 mm, and the fine

Table 1 Chemical compositions of GGBFS (mass %)

Component	SiO_2	Al_2O_3	Fe_2O_3	CaO	MgO	K_2O	Na_2O	TiO_2	Mn_2O_3
GGBFS	41.66	13.96	1.49	34.53	5.53	0.97	0.49	0.58	0.35

Table 2 Characteristics of used steel rebars

Bars diameter (mm)	Yield strength (MPa)	Tensile strength (MPa)	Elongation percentage (%)	Ribs height (mm)	Ribs spacing (mm)
12	473	644	25.2	1.1	7.8
16	540	690	21.3	1.1	10.3
22	572	745	20.8	1.6	13.0

aggregate (natural sand) was with fineness modulus of 2.77. The alkaline activator was a mixture solution of sodium silicate and sodium hydroxide. The solution of sodium hydroxide solution was prepared by dissolving flakes of pure sodium hydroxide in potable water, while the sodium silicate solution was obtained from a local supplier. The used sodium hydroxide flakes had a chemical composition of 60.25% Na_2O and 39.75% H_2O, while the chemical composition of the used sodium silicate solution was 31.00% SiO_2, 11.98% Na_2O, and 57.00% H_2O. The rebars used to investigate the bond behavior were steel ribbed bars with properties as shown in Table 2. The mix proportions for the used AASC and its characteristics are shown in Table 3.

2.2 Test Specimens

Nine beam-end specimens with of 200 mm in wide, 300 mm in height, and 600 mm in length were investigated. Both of tension and compression reinforcement was two deformed rebars with diameter of 12 mm positioned in the beam corners, while the shear reinforcement was stirrups with 8 mm in diameter with spacing of 125 mm. The configuration of test specimen was determined to fulfill the requirements of the ASTM A 944 (2005). Fig. 1 illustrates the configuration and presents the dimensions of the used specimens. One tested steel rebar was placed in the tension side for each test specimen; the bottom concrete cover of the tested rebar was 50 mm, while the side concrete cover was 100 mm, and these covers were kept constants for all tested specimens. A plastic tube was used to make the first 50 mm distance from the tested rebar, measured from the loaded end

Table 3 Mix proportions and properties of the used AASC

GGBFS	SS[a]	SH[b]	Add. water	F.A.[c]	C.A.[d]	Compressive strength (MPa)	Slump (mm)
450	131	41	112	547	1093	44.0	230

[a] SS = Na_2SiO_3, [b]SH = NaOH, [c]F.A. = fine aggregate, [d]C.A. = coarse aggregate.

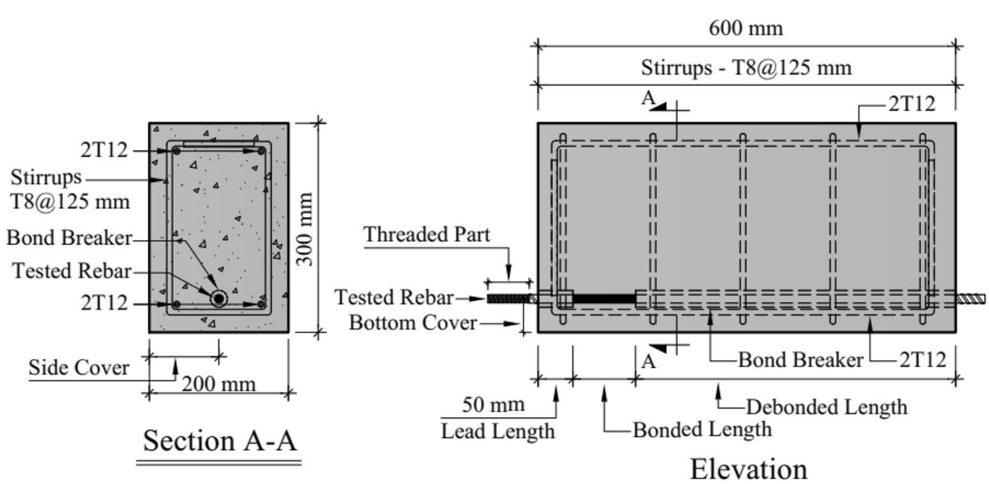

Fig. 1 Configuration and dimensions of beam-end test specimen

Fig. 2 Shape of reinforcement cage and tested rebar in the mold

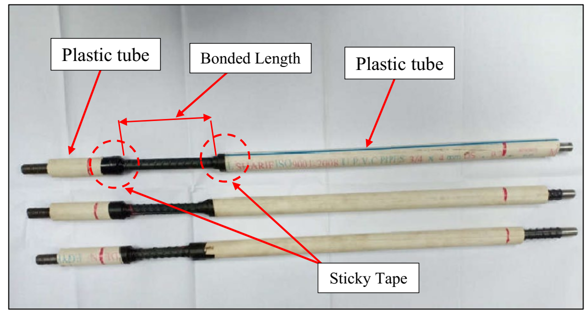

Fig. 3 Shape of tested rebars before placing in the mold

concrete surface, debonded. This distance is called the lead length which should be achieved to avoid the possible conical failure. The tested bonded length, which calculated according to the investigated bond length to diameter (L/d) ratio, followed the lead length (50 mm distance), and then the remaining part of the tested rebar was debonded using also plastic tube as shown in Fig. 1.

2.3 Preparation and Testing of Specimens

Mixing criteria implemented in this work for the alkali-activated concrete initiated with mixing the dry materials, GGBFS and aggregates, in the pan of mixer for about 1 min. Then, the alkaline activator was added to the dry mixture and then mixing for around 4 min until the mixture became homogeneous. The preparation process of the alkaline activator was by mixing the sodium hydroxide flakes, sodium silicate solution and potable water for around 1 h before adding it to the dry mixture until its average temperature was about 30 °C. Before casting, the cage of reinforcement bars was positioned in the mold and then the tested steel rebar oriented horizontally in its proper position as presented in Fig. 2. Plastic tubes and sticky tape were used to make the bond breakers for the tested rebars to achieve the required bonded length for testing as illustrated in Fig. 3. The test specimens were demolded after 24 h from casting, and then kept in the laboratory at the ambient temperature (25 ± 2 °C) and relative humidity (50 ± 5%) until the testing date.

For the specimens that were exposed to elevated temperatures, their apparent parts of their tested rebars were painted with an anti-rust material to keep it from being corroded by elevated temperatures. After painting the rebars, they were covered with a heat-insulation material (ceramic fiber fabrics) to prevent the rapid transfer of heat to the embedded part of rebars inside the concrete and also so that its tensile strength would not be affected by the elevated temperatures. Fig. 4 shows the beam-end specimens after preparing the rebars.

The configuration of the test setup of specimens is illustrated in Figs. 5 and 6. The reaction steel plate was positioned at the specimen bottom (compression side) to achieve uniform distribution for the induced stresses. The applied tension force acting on the tested steel rebar generated by using a hydraulic jack with capacity of 300 kN. The test specimen was fixed in its position by anchoring it to the reaction steel frame using two steel plates with four steel threaded bars and nuts. The values of applied tension loads were measured by using a special load cell positioned between the hydraulic jack and test specimen which connected to specimen by a threaded part in the outer part of the tested rebar and connected to the hydraulic jack using an external threaded bar. Slippage that occurred in the free end of the tested steel rebar was recorded by using LDVT.

The bond strength, τ_u, was determined based on the obtained ultimate load, P_u, resisted by the tested steel rebar by using Eq. (1) (Castel & Foster, 2015):

$$\tau_u = \frac{P_u}{\pi \cdot \emptyset \cdot L}, \tag{1}$$

where τ_u = bond strength (MPa); $\emptyset$ = diameter of tested rebar (mm); L = bonded length of tested rebar (mm); P_u = ultimate load resisted by the tested rebar (pull-out) (N).

The axial tensile stress, σ_u, in the tested rebar corresponding to its ultimate bond strength, was determined by using Eq. (2):

$$\sigma_u = \frac{P_u}{\pi . \emptyset^2 / 4}, \tag{2}$$

where σ_u = tensile stress in the tested rebar (MPa); $\emptyset$ = diameter of tested rebar (mm); P_u = ultimate load resisted by the tested rebar (pull-out) (N).

2.4 Test Matrix

In this study, pulling-out testing was performed on beam-end specimens to investigate the bond behavior. The beam-end technique was selected because of its simulation to the actual bond between the rebars and

(a) Beam-end specimens after painting the rebars with the anti-rust material.

(b) Beam-end specimens after covering the rebars with the heat-insulation material.

Fig. 4 Preparation of beam-end specimens before exposure to the elevated temperature

concrete in the reinforced concrete elements that subjected to flexure (Shamseldein et al., 2018).

Taguchi method was applied to design the experiments to reduce the number of tested beams while preserving the possibility of interpreting and analyzing the test results for the studied different factors and levels. Three factors related to bond behavior with three levels for each factor were considered. Table 4 presents the parameters and levels that employed in the Taguchi method. By using Taguchi design and according to L9 array, nine beams were obtained as shown in Table 5.

The code of specimens presented in Table 5 refers to the studied parameters. The first part describes the rebar diameter, the second part describes the exposure condition, and the last part describes the development length-to-diameter ratio. For example, specimen (D12-T300-6) refers to a specimen reinforced by 12-mm-diameter rebar, exposed to elevated temperature of 300 °C, and the applied development length-to-diameter ratio is 6.

2.5 Heating Regime

After 28 days of curing, the prepared test specimens were exposed to elevated temperatures in an electric furnace with a temperature capacity of 1200 °C as shown in Fig. 7. Six specimens were exposed to two degrees of temperature (300 and 600 °C), three specimens for each temperature degree. The heating rate of the furnace was 5 °C/min. After reaching the required temperature, the heated specimens kept at this temperature in the furnace for a period of 1.5 h to achieve the temperature homogenization in the specimens. Then, the heated specimens were cooled naturally by opening the ventilation hole in the furnace to ambient temperature. Fig. 8 presents the time–temperature regime of all targeted elevated temperatures that applied on the test specimens.

3 Results and Discussion

To determine the concrete compressive strength of the tested beams, core specimens were extracted from the beams after testing from a location far from the failure positions, using a core cutter device as shown in Fig. 9. Table 6 presents the test results for the compressive strength of tested specimens before and after exposing to the elevated temperatures. Moreover, Table 7 shows the results of all test specimens. Ultimate bond strength, τ_u, free-end slippage that is corresponding to the obtained ultimate bond stress, S_u, maximum tension stress induced in the tested steel rebar that is corresponding to the ultimate bond strength, σ_u, as a percentage of the maximum tensile strength of the tested steel rebar, f_u, the ascending branch slope, $K_a = \tau_u / S_u$, and the observed modes of failure are summarized in Table 7.

3.1 Elevated Temperatures Damage

The damage caused by applying the elevated temperatures were evaluated for all heated test specimens by performing the unit weight, compressive strength and ultrasonic-pulse velocity tests on specimens extracted from the beams after testing. Table 8 presents the results of all carried-out tests. Percentage of unit weight loss, compressive strength loss and ultrasonic-pulse velocity

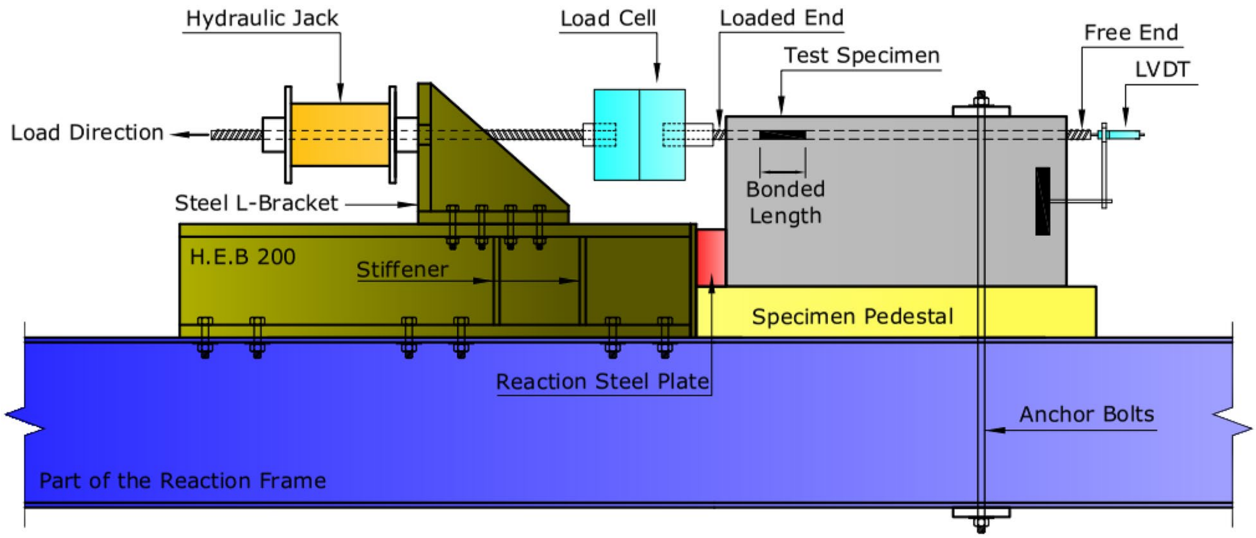

Fig. 5 Schematic for the beam-end specimen test setup

Fig. 6 Setup of beam-end specimen test

Table 4 Parameters and levels employed in Taguchi design

Parameters	Level 1	Level 2	Level 3
Bar diameter (mm)	12	16	22
Temperature (°C)	25	300	600
Bond length to diameter (L/d)	4	6	8

loss were calculated and plotted as presented in Fig. 10. Also, the heated specimens were inspected visually after removing them from the furnace, where tiny cracks scattered on the surface with slight thermal spalling for the specimens' edges were observed in all heated specimens.

3.2 Mode of Failure and Cracking Pattern

Cracking patterns resulting at failure for all test specimens are presented in Fig. 11. The failure mode of all beams was splitting mode failure, where a single crack started at the loaded end of specimen and propagated in the longitudinal direction of the tested rebar towards the specimen free end, then this longitudinal single crack was branched out into two cracks towards the edges of the tested specimen at the end of the bonded length of the tested rebar. It can be said that a typical cracking pattern and failure mode were obtained for the tested specimens are as illustrated in Fig. 12. The obtained crack pattern was similar to that of OPC concrete under pull-out load which agreed with what found by Sarker (2011). There was no significant difference observed in the obtained cracking pattern and failure mode due to the elevated temperature exposure. This can be attributed to the high stability, which means no significant changes occurred, of the AAC products, which are generated due to the hydration and polymerization of its binder, in the presence of alkaline activator, at elevated temperatures. Also, the obtained porous micro-structure in AAC makes it have better performance at elevated temperatures (Jiang et al., 2020).

Table 5 Test matrix

Ser	Specimens designation	Bar diameter (mm)	Temperature (°C)	Bond length to diameter (L/d)
1	D12-T25-4	12	25	4
2	D12-T300-6		300	6
3	D12-T600-8		600	8
4	D16-T25-8	16	25	8
5	D16-T300-4		300	4
6	D16-T600-6		600	6
7	D22-T25-6	22	25	6
8	D22-T300-8		300	8
9	D22-T600-4		600	4

(a) Empty furnace (b) Specimens set up in the furnace

Fig. 7 The used electric furnace

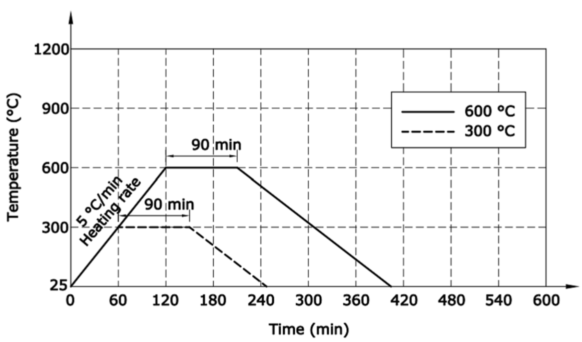

Fig. 8 Applied time–temperature regime

3.3 Bond Stress–Slip Relationships

Fig. 13 presents the relationships between bond stress and slippage that occurred at the free end of all tested specimens. These relationships were separated into three groups as illustrated in Figs. 14, 15 and 16 according to the rebar diameter to clarify the relationships and the differences between them. The bond stress–free-end slip relationships of “D12-T25-4”, “D12-T300-6” and “D12-T600-8” specimens are presented in Fig. 14, while the bond stress–free-end slip relationships for “D16-T25-8”, “D16-T300-4” and “D16-T600-6” specimens are presented in Fig. 15, and the bond stress–free-end slip

(a) Extracted specimens (b) Extracted specimen in compression test

Fig. 9 Extracting cylindrical specimens and testing them in compression

Table 6 Test results of compressive strength

Ser	Exposure temperature (°C)	Compressive strength	
		results (MPa)	Referring to the ambient (%)[a]
1	Ambient (25)	34.9	100
2	300	28.7	82
3	600	18.6	53

[a] Represents the residual compressive strength after exposure to elevated temperature as a percentage from the compressive strength at ambient temperature.

Table 8 Tests results for the evaluation of beam-end specimens

Ser	Exposure temperature (°C)	Unit weight (kg/m^3)	Compressive strength (MPa)	Pulse velocity (m/s)
1	25	2432	34.9	4620
2	300	2365	28.7	3714
3	600	2264	18.6	1188

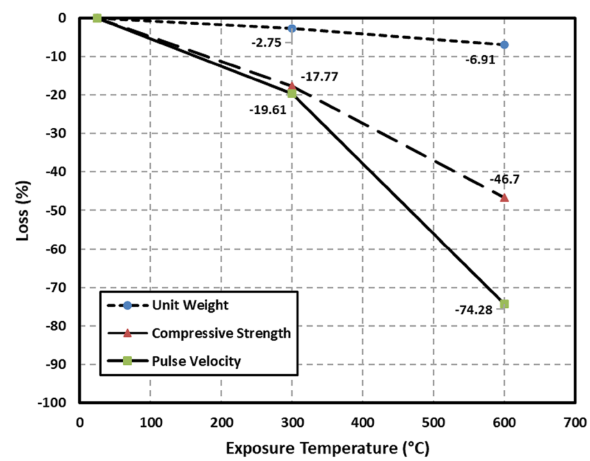

Fig. 10 Percentage of unit weight loss, compressive strength loss and ultrasonic-pulse velocity loss for all extracted specimens

relationships for "D22-T25-6", "D22-T300-8" and "D22-T600-4" specimens are presented in Fig. 16.

As shown in Table 7 and Figs. 14, 15 and 16, the bond stress–slip relationships of the specimens that were exposed to 25 °C (ambient temperature) demonstrated a steep ascending branch at the low values of slippage, then followed by a soft increasing up to the maximum bond stress. These specimens had achieved the highest values for the ascending branch slope. For the specimens exposed to elevated temperatures, their bond stress–slip relationships showed less steep ascending branches up to the maximum bond stress than those of specimens at ambient temperature. This result is clearer from the values of ascending branch slopes reported in Table 7. It can be seen that by increasing the temperature degree of exposure, the value of ascending branch slope was decreased. Also, it was noticed that the exposure to elevated temperatures caused a significant reduction in the maximum bond stress, and an increase in the free-end slippage that was corresponding to the maximum bond stress. Moreover, test specimens that were exposed to elevated temperatures achieved the lowest slopes for the ascending branch.

To surmount the difficulty of investigating how the different parameters affect the values of τ_u and S_u, program of Minitab was employed to determine the signal-to-noise (S/N) ratio for all considered parameters affect both of τ_u and S_u as shown in Figs. 17 and 18, respectively. Also, ANOVA approach was used by employing the program of Qualitek-4 to calculate the percentage of participation and optimum level of all considered

Table 7 Test results of beam-end specimens

Ser	Code	τ_u (MPa)	S_u (mm)	σ_u/f_u (%)	K_a (N/mm^3)	Failure mode
1	D12-T25-4	15.01	0.2111	37.30	71.10	Splitting
2	D12-T300-6	13.46	0.4491	50.15	29.97	
3	D12-T600-8	10.53	0.7030	52.30	14.98	
4	D16-T25-8	15.56	0.1603	72.17	97.07	
5	D16-T300-4	10.97	0.5745	25.44	19.09	
6	D16-T600-6	8.54	0.8550	29.70	9.99	
7	D22-T25-6	14.01	0.3570	45.13	39.24	
8	D22-T300-8	11.29	0.5709	48.49	19.78	
9	D22-T600-4	6.98	1.1145	14.99	6.26	

τ_u = the ultimate bond strength ($\tau_u = \frac{P_u}{\pi \emptyset L}$); S_u = free-end slippage that is corresponding to the obtained ultimate bond strength; σ_u = tensile stress in the tested steel rebar that is corresponding to the obtained ultimate bond strength ($\sigma_u = \frac{P_u}{\pi \emptyset^2/4}$); f_u = maximum tensile strength of the tested steel rebar; K_a = the ascending branch slope of bond stress–slip curve ($K_a = \tau_u/S_u$).

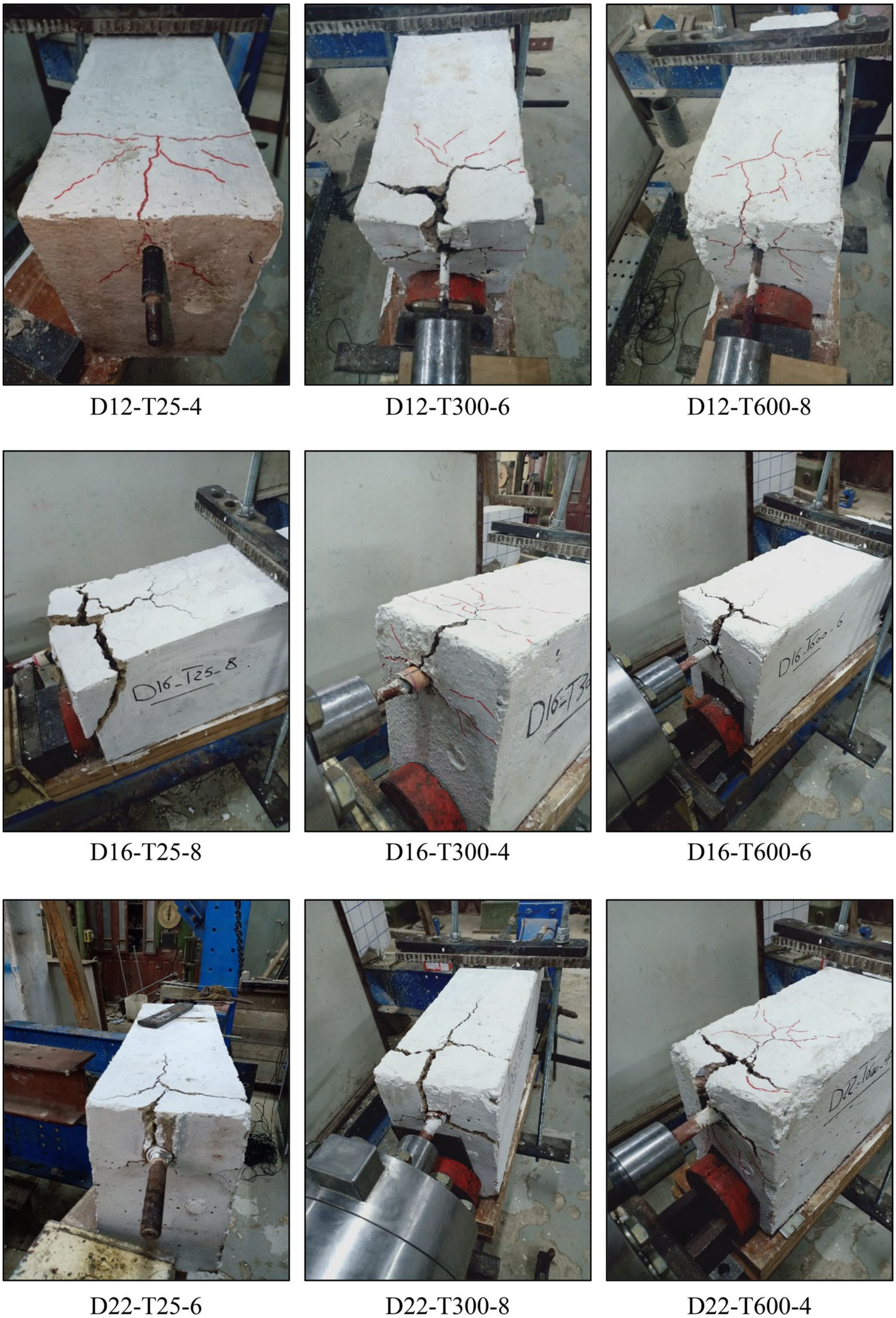

Fig. 11 Modes of failure and cracking patterns for all tested beam-end specimens

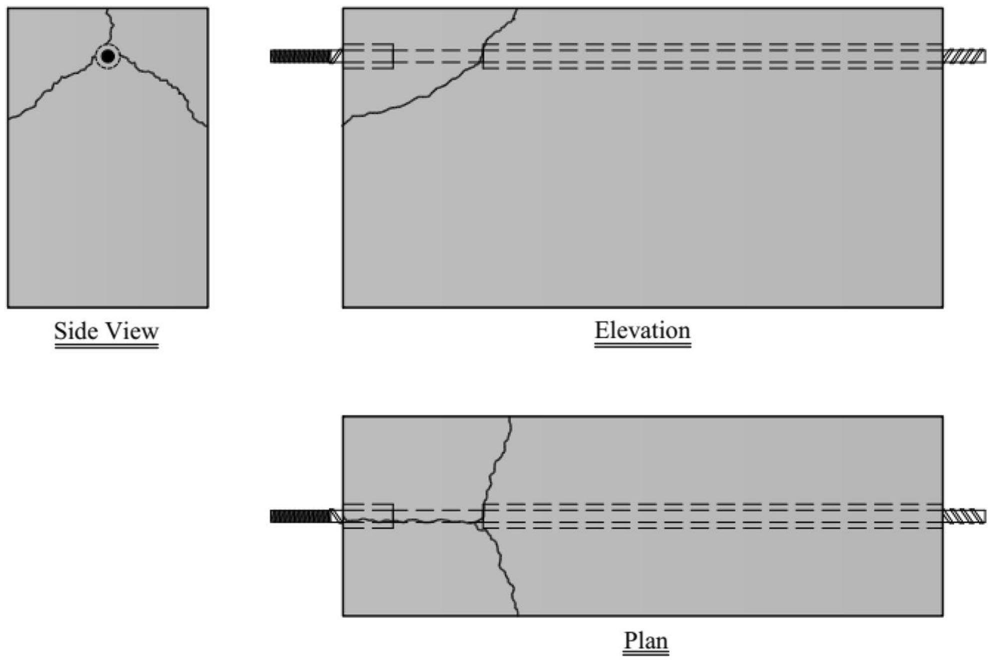

Fig. 12 Typical cracking pattern of the tested beam-end specimens

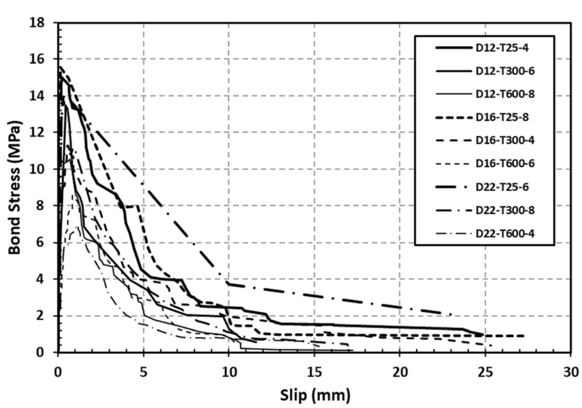

Fig. 13 Bond stress–slip relationships of all test specimens

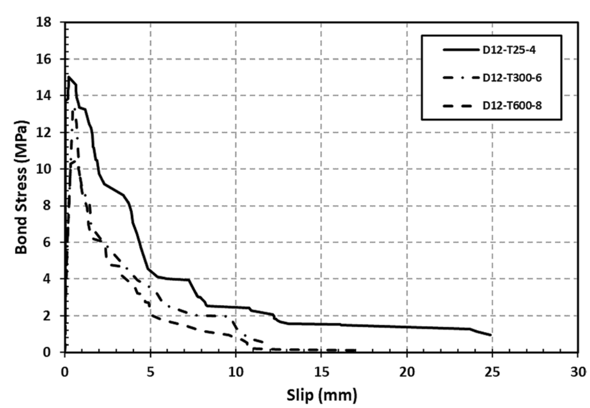

Fig. 14 Bond stress–slip relationships of the case of 12-mm-diameter rebars

parameters on both of τ_u and S_u as given in Tables 9 and 10, respectively.

It can be observed from Fig. 17 and Table 9 that the exposure temperature was the most significant parameter that affects the value of "τ_u". The participation percentage was 83.27% and the optimum level was 25 °C. This means that by increasing the exposure temperature, the maximum bond stress was decreased, which can be attributed to the obtained decrease in the compressive strength and tensile strength after exposing to the elevated temperatures. The degradation in τ_u when exposing to elevated temperature above 300 °C was more significant. The reduction in S/N ratio at temperatures of 300 °C and 600 °C from the ambient temperature of 25 °C was 8.32% and 20.40%, respectively. This is agreed with what reported by H.Y. Zhang et al. (2018) (Zhang et al., 2018).

The bar diameter is the second significant parameter with a participation percentage of 10.76% and the 12 mm bar diameter (the lowest diameter) was the optimum level, as presented in Table 9. This demonstrates that the bond behavior of small-diameter rebars was better than that of large-diameter rebars as shown in Fig. 17. The improvement in the bond behavior occurred due to more favorable ratio between

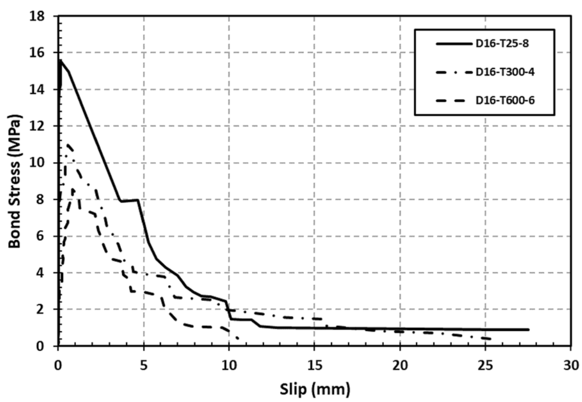

Fig. 15 Bond stress–slip relationships of the case of 16-mm-diameter rebars

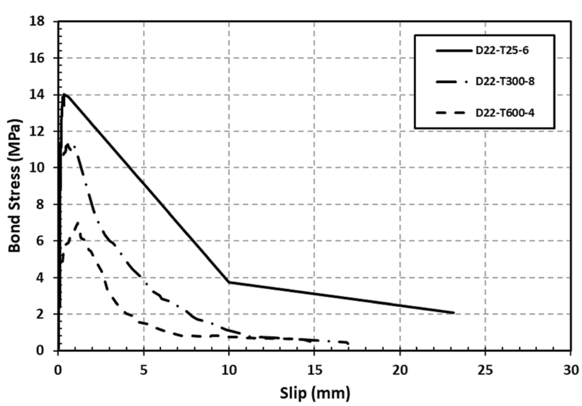

Fig. 16 Bond stress–slip relationships of the case of 22-mm-diameter rebars

bond surface area and cross-sectional area of rebars (Bamonte et al., 2004; Wu & Zhao, 2013).

The L/d ratio was achieved the lowest value for the percentage of participation, 4.65%, with optimum level of 8. This indicates that by increasing the L/d ratio, the τ_u was increased as shown in Fig. 17. The increase of τ_u due to increasing the L/d ratio was not significant. The increase in S/N ratio for L/d of 6 was 4.80% higher than that for L/d of 4, while the increase in S/N ratio for L/d of 8 was 6.76% higher than that for L/d of 4. This indicates that increasing the L/d ratio does not increase τ_u significantly which agreed with what found by Eligehausen et al., (1982), Xu (1990) and Harajli et al., (2004).

From Fig. 18, it can be observed that the S_u decreased by increasing of both rebar diameter and exposure temperature and increased by increasing of the L/d ratio. As reported in Table 10, the most significant factor on S_u was the exposure temperature, then rebar diameter and finally the L/d ratio with percentages of participations of 82.81%, 10.74% and 4.85%, and with optimum levels of 25 °C, 12 mm and 8, respectively.

4 Analytical Study

4.1 Available Models

There is a need to verify the bond behavior of AASC using the available bond models used for OPC concrete to see how accurate these models predict the bond behavior of AASC. Two common models were utilized to predict the bond behavior for the conventional concrete with rebars were used in this analytical study. The first one was in the CEB-FIP model (Comite EURO—International du Beton, 1990) while the second one was the model that proposed by Maree 2014 (Farghal Maree & Hilal Riad, 2014). These two models were used to compare the experimental results of bond behavior with those obtained analytically from the aforementioned two models.

In CEB-FIP, the relationship between bond stress and slippage is defined by a set of equations, which are based on several parameters: concrete compressive strength, rebar diameter, type of reinforcement (smooth or deformed), confinement conditions and bond conditions. The analytical relationship of bond stress–slip in accordance with CEB-FIP model is presented in Fig. 19.

In Fig. 19, the first branch, ascending, which is a non-linear part, represents the phase in which the ribs, on the surface of rebars, penetrate and interlock through the mortar matrix of concrete, characterized by microcracking and crushing locally. Maximum slip of this first branch (ascending) is considered the characteristic slip which denoted as S_1. The constant horizontal part, which occurs in case of confined concrete only, is referring to the shearing and advanced crushing of concrete between the ribs of rebar. The maximum slip of this part is denoted as S_2. This constant part is followed by descending branch which is referring to the decrease in the bond resistance because of the induced cracks occurred in the longitudinal direction of rebars due to splitting. The maximum slip of this descending branch is denoted as S_3. The lower horizontal part refers to the residue of bond strength, which is retained due to minimal transverse reinforcement, while maintaining a particular integrity intact degree.

For monotonic loading, bond stress between concrete and rebar can be determined as a function of the relative displacement, S, according to Eqs. (3) to (6). The values of parameters in these equations are defined in Table 11:

$$\tau = \tau_{\max}\left(\frac{S}{S_1}\right)^{\alpha}, \quad 0 \leq S \leq S_1, \tag{3}$$

$$\tau = \tau_{\max}, \quad S_1 < S \leq S_2, \tag{4}$$

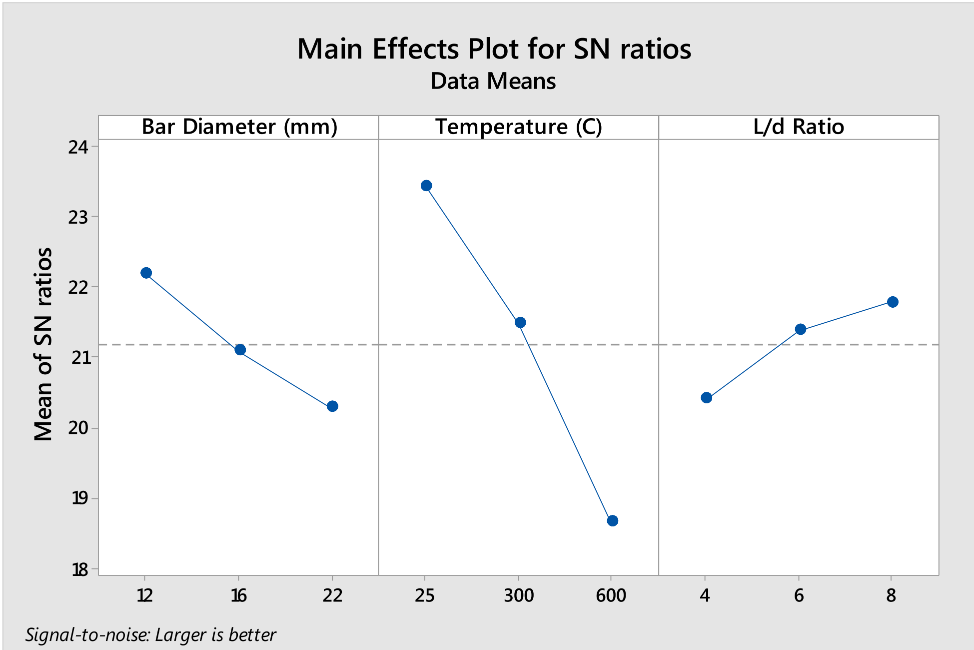

Level	Bar Diameter (mm)	Temperature (C)	L/d Ratio
1	22.19	23.43	20.40
2	21.09	21.48	21.38
3	20.29	18.65	21.78
Delta	1.90	4.78	1.38
Rank	2	1	3

Fig. 17 The significance of main parameters affecting "τ_u" (Minitab program)

$$\tau = \tau_{\max} - \left(\tau_{\max} - \tau_f\right)\left[\frac{S - S_2}{S_3 - S_2}\right], \quad S_2 < S \leq S_3, \tag{5}$$

$$\tau = \tau_f, \;\; S_3 < S. \tag{6}$$

Maree 2014 investigated the bond characteristics for two types of conventional concrete (Normal Weight Concrete "NWC" and Light Weight Concrete "LWC") with steel rebars using pull-out test for both beam-end and lollipop specimens. This study investigated the bond of straight, deformed, and unanchored steel rebars with LWC in flexural elements with investigating the validity of both available design codes and bond models to predict the bond behavior for LWC. The main parameters considered in this study were concrete type (NWC and LWC), diameter of rebars (12, 16 and 22 mm) and bonded length-to-diameter ratio (2, 3 and 4).

At the end of this study, Maree proposed modifications in the main parameters of the CEB-FIP model to consider the effect of both concrete type and bar diameter on the bond stress–slippage relationship. These modifications were in characteristic slippages (S_1) and (S_2) and bond strength ($\tau_{\max}$) as presented in Table 11.

4.2 Comparative Study

Comparison between the two aforementioned models with the obtained experimental results was conducted. The results of this comparison are presented in Figs. 20, 21 and 22. It was observed that the CEB-FIP model demonstrated underestimated values for the bond strength and revealed bond–slip relationships with steeper descending branches than experimental results at both

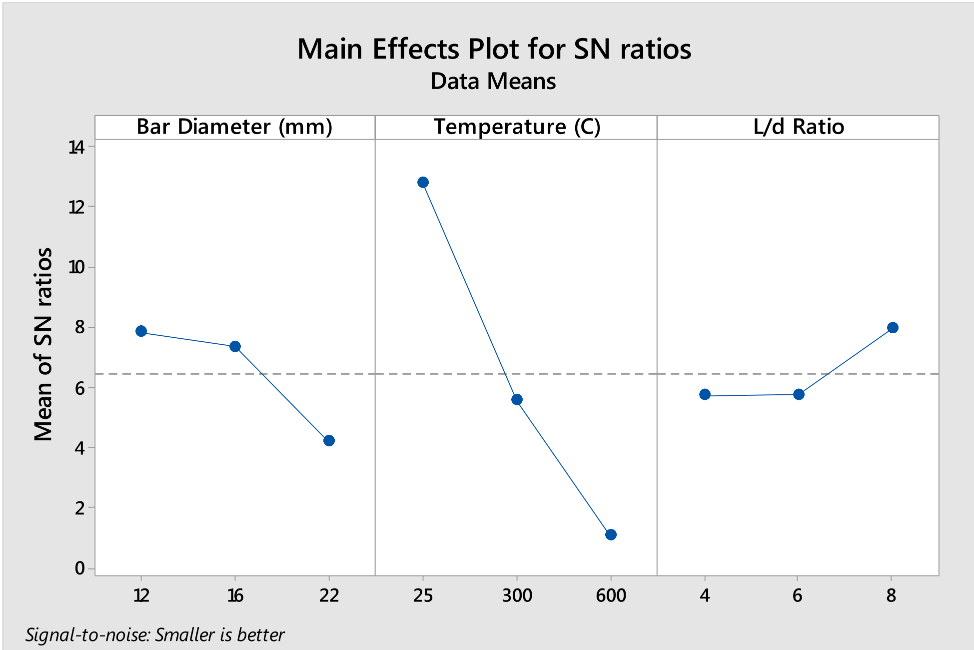

Level	Bar Diameter (mm)	Temperature (C)	L/d Ratio
1	7.841	12.786	5.716
2	7.359	5.545	5.753
3	4.213	1.082	7.944
Delta	3.628	11.704	2.228
Rank	2	1	3

Fig. 18 The significance of main parameters affecting "S_u" (Minitab program)

Table 9 Percentage of participation and optimum level for all considered parameters on τ_u

Parameter	Bar diameter (mm)	Temperature (°C)	L/d
Percentage of participation (%)	10.76	83.27	4.65
Optimum level	12	25	8

Table 10 Percentage of participation and optimum level for all considered parameters on S_u

Parameter	Bar diameter (mm)	Temperature (°C)	L/d
Percentage of participation (%)	10.74	82.81	4.85
Optimum level	12	25	8

ambient and elevated temperature. However, it was observed that the value of bond strength obtained from CEB-FIP model approached the experimental results with increasing the exposure temperature. The model proposed by Maree 2014 gave over-estimated values for the bond strength and gave bond–slip relationships with steeper descending branches than the obtained experimental results at ambient and elevated temperature.

This comparison showed a high deviation between the experimental results with those obtained analytically from the aforementioned two models. This means that, these models are of low accuracy to predict the bond behavior of AASC which attributed to the difference between the conventional concrete and the AASC in many aspects such as components, hydration products, manufacturing technique and general behavior. That is

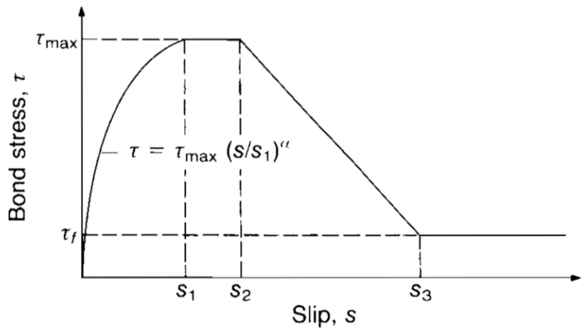

Fig. 19 Bond stress–slip relationship (CEB-FIP model) (Comite EURO—International du Beton, 1990)

Table 11 Defining parameters of the bond stress–slippage relationship

Parameters	CEB-FIP	Maree 2014
S_1(mm)	0.60	$0.11 \times e^{0.054\emptyset}$
S_2(mm)	0.60	25
S_3(mm)	1.00	1.00
α	0.40	0.40
τ_{max}(MPa)	$2\sqrt{f_c'}$	$10.4 \times \emptyset^{-0.35}\sqrt{f_c'}$
τ_f(MPa)	$0.15\tau_{max}$	$0.15\tau_{max}$

*$\emptyset$ = rebar diameter (mm)

**f_c' = concrete compressive strength (MPa)

why a modified model is proposed to predict AASC bond behavior with a higher accuracy.

4.3 Proposed Modified Model

The main target of this analytical study was to introduce a proposed modified model in order to predict a complete bond behavior between ambient cured AASC and steel rebars more accurate than the aforementioned models used for conventional concrete.

To improve the prediction level of AASC bond behavior, modifications were proposed on the main parameters of CEB-FIP model based on the technique of best fitting for the obtained experimental results, these modifications are shown in Table 12. These modifications were in the bond strength (τ_{max}) and the characteristic slippage (S_3). The bond strength increased from $2\sqrt{f_c'}$ to $2.5\sqrt{f_c'}$, as the AASC showed bond strength higher than the conventional concrete as reported in the literature and as obtained from the experimental results of this research work. The characteristic slippage (S_3) modified from 1.00 mm to the clear rib spacing of rebars to make the descending branch less steep.

Comparison between the results of proposed model, and both of the obtained experimental results and the results obtained analytically from the aforementioned two models was conducted at both ambient temperature (25 °C) and elevated temperatures of 300 °C and 600 °C as shown in Figs. 23, 24 and 25, respectively. It was noted that the proposed modified model matched well the experimental results at ambient temperature (25 °C). This can be attributed to that the criteria used in the study to modify the model were based on the findings of previous studies conducted on AAC samples at ambient temperature, due to the limited studies found for elevated temperatures. Also, it was observed that the proposed modified model gave over-estimated bond–slip relationships for all specimens that were exposed to elevated temperatures except 12-mm-diameter rebars specimens, which the proposed modified model matched well their ascending branches up to the maximum bond strength and then gave over-estimated descending branches. This means that there is a need for further investigation to reach a modification factor for the main parameters of the bond–slip relationship, especially for τ_{max} and S_3, to be used in the case of exposure to elevated temperatures. After considering the results obtained from this study, this factor is likely to be a reduction factor. Also, it is recommended for this modification factor to be linked to the used rebars diameter.

Table 12 Modified defining parameters of the bond stress–slippage relationship

Parameters	CEB-FIP	Maree 2014	Proposed model
S_1(mm)	0.60	$0.11 \times e^{0.054\emptyset}$	0.60
S_2(mm)	0.60	25	0.60
S_3(mm)	1.00	1.00	Clear rib spacing
α	0.40	0.40	0.40
τ_{max}(MPa)	$2\sqrt{f_c'}$	$10.4 \times \emptyset^{-0.35}\sqrt{f_c'}$	$2.5\sqrt{f_c'}$
τ_f(MPa)	$0.15\tau_{max}$	$0.15\tau_{max}$	$0.15\tau_{max}$

5 Conclusions

Both of experimental and analytical investigation for the bond behavior between AASC and steel rebars after exposing to elevated temperatures was presented and discussed. Based on analyzing and discussing the obtained results, the following conclusions can be drawn:

- Failure mode for all beam-end specimens was by splitting. There was no significant difference observed in the obtained cracking pattern or failure mode due to exposing to the elevated temperatures.
- The degradation level of bond strength after exposing to elevated temperatures above 300 °C was significant. Generally, bond strength decreased, and

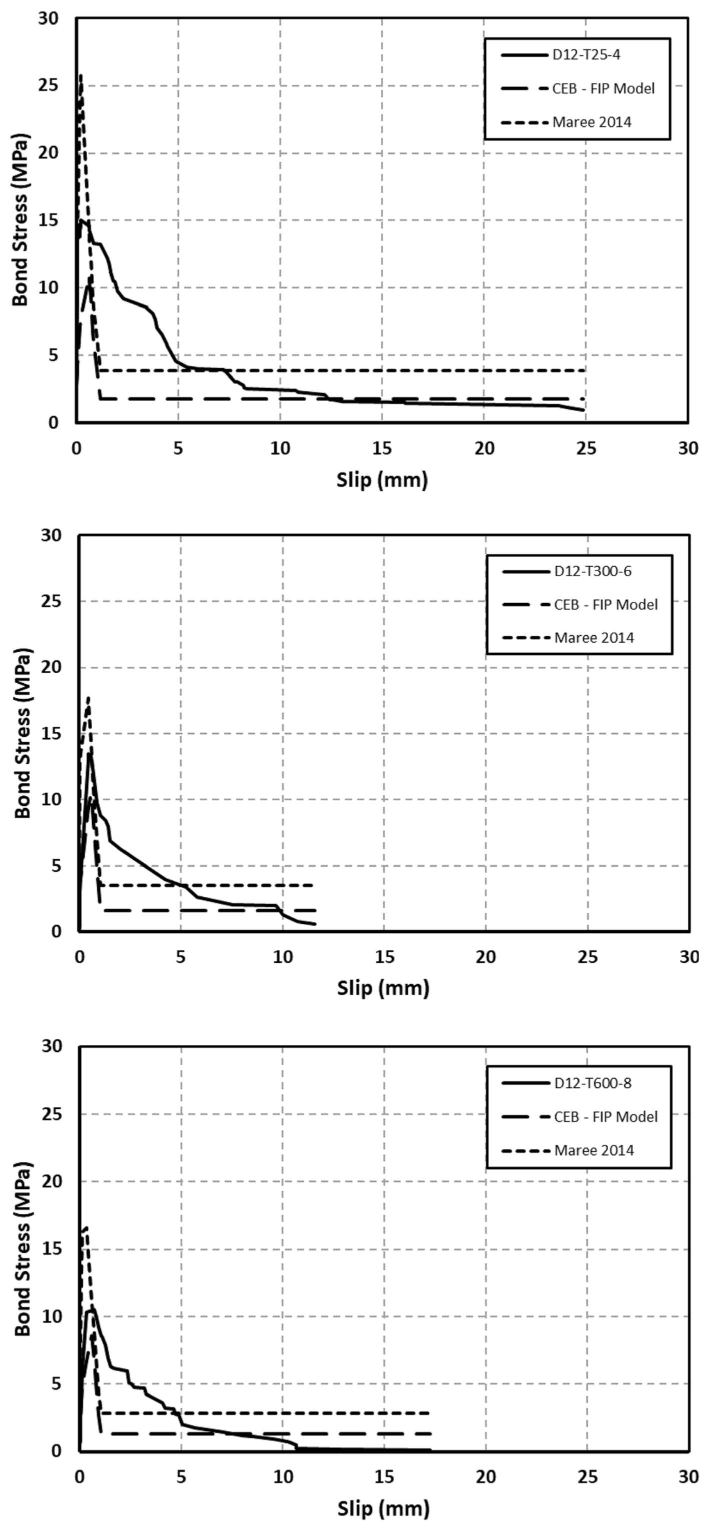

Fig. 20 Analytical versus experimental bond–slip curves (specimens of 12-mm-diameter rebars)

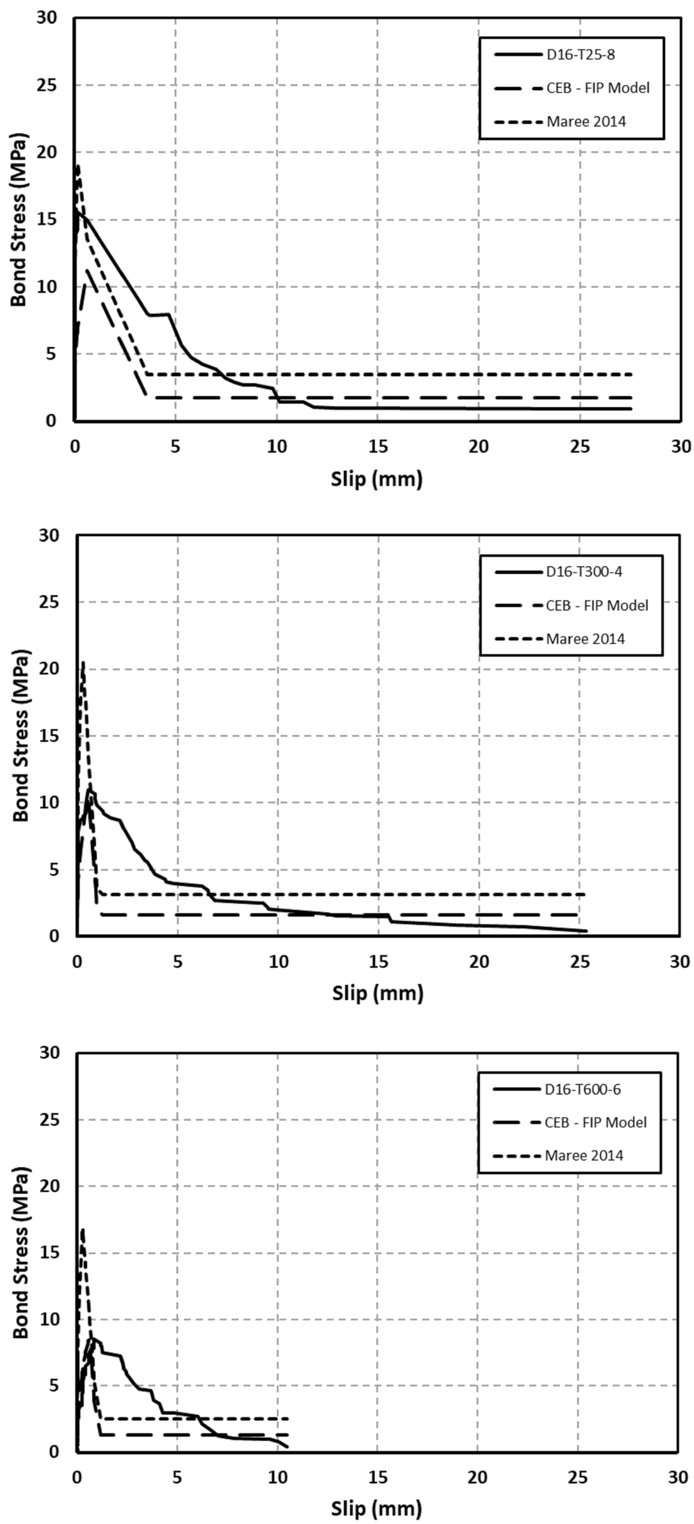

Fig. 21 Analytical versus experimental bond–slip curves (specimens of 16-mm-diameter rebars)

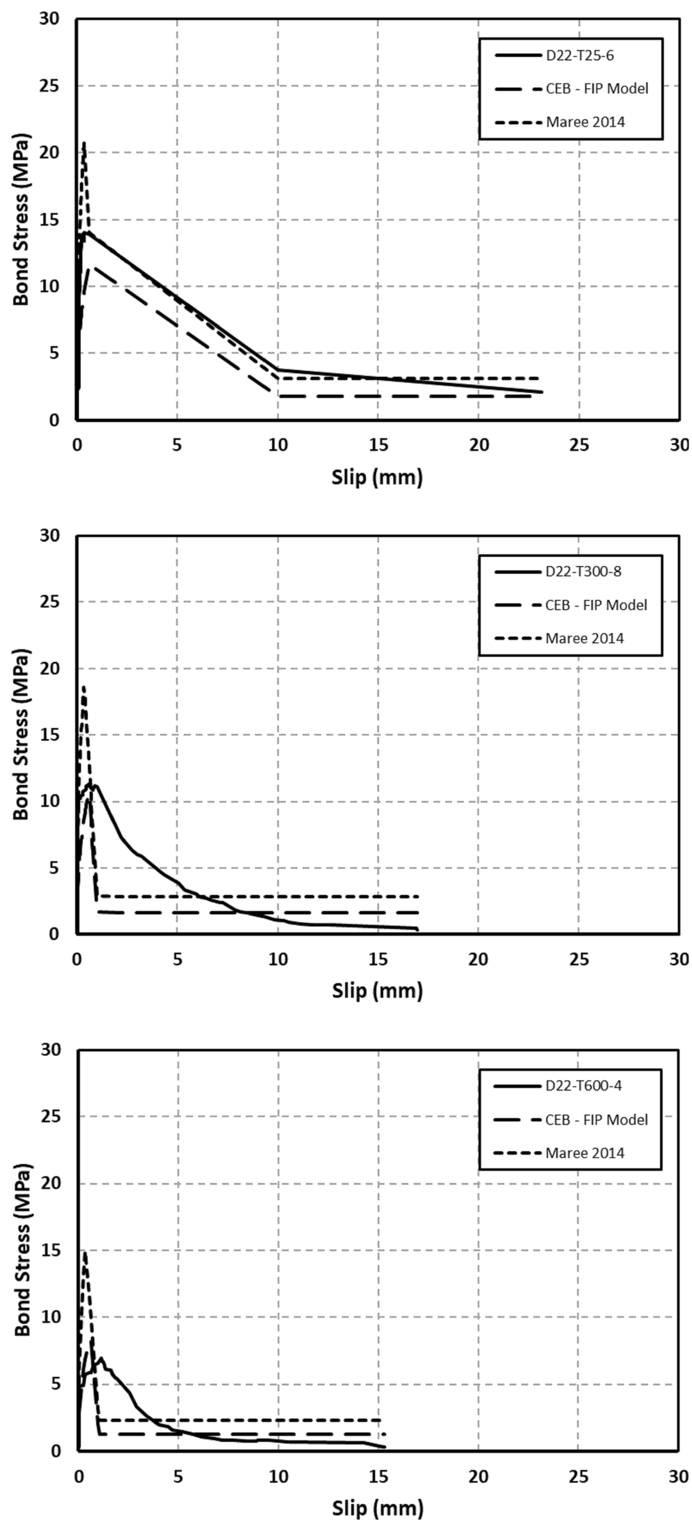

Fig. 22 Analytical versus experimental bond–slip curves (specimens of 22-mm-diameter rebars)

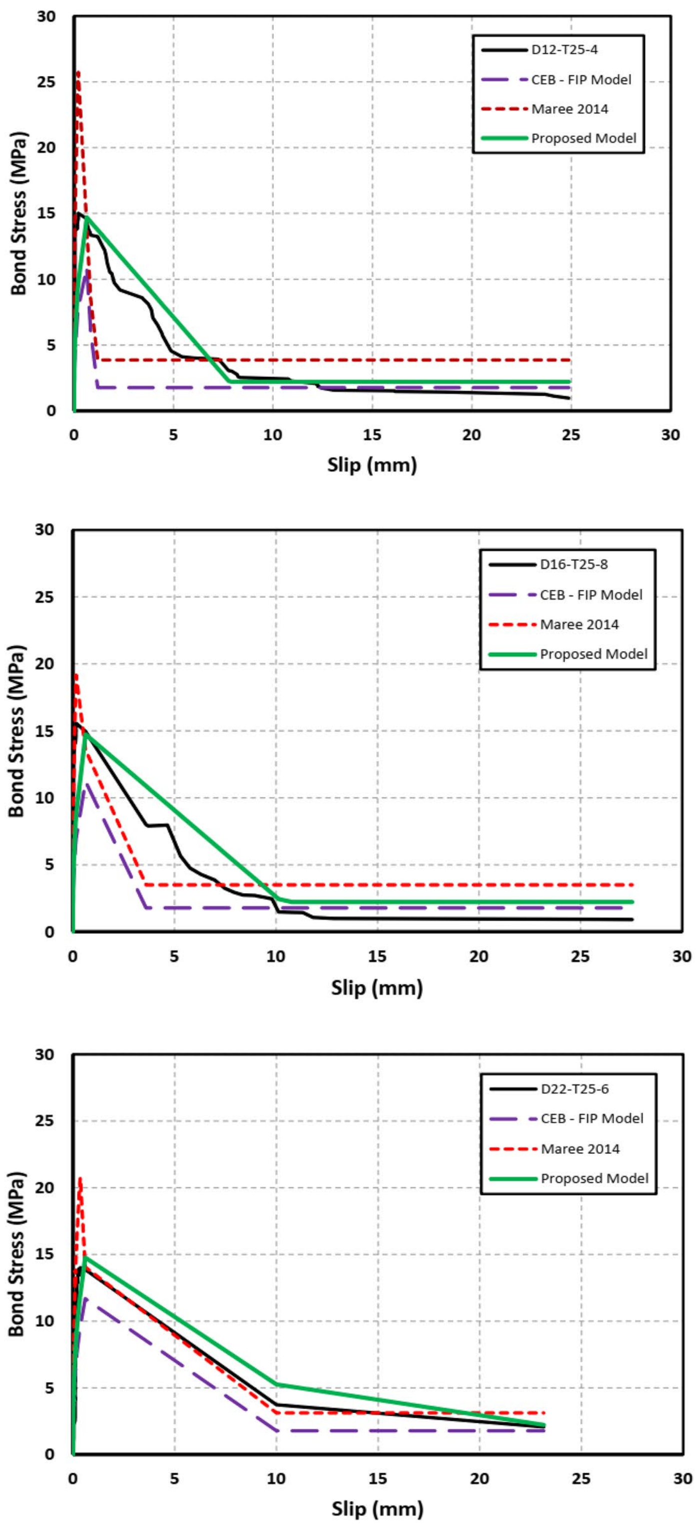

Fig. 23 Proposed analytical versus experimental bond–slip relationships (ambient temperature of 25 °C)

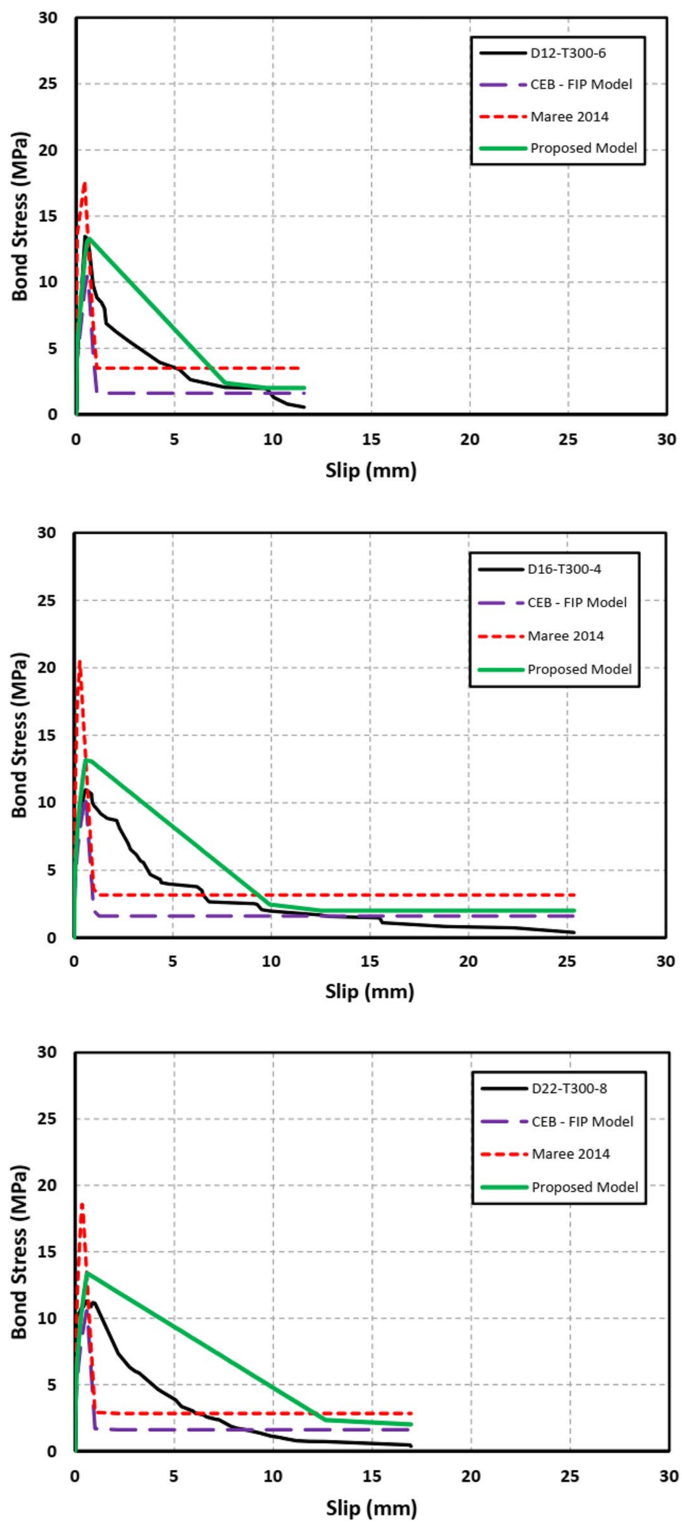

Fig. 24 Proposed analytical versus experimental bond–slip relationships (elevated temperature of 300 °C)

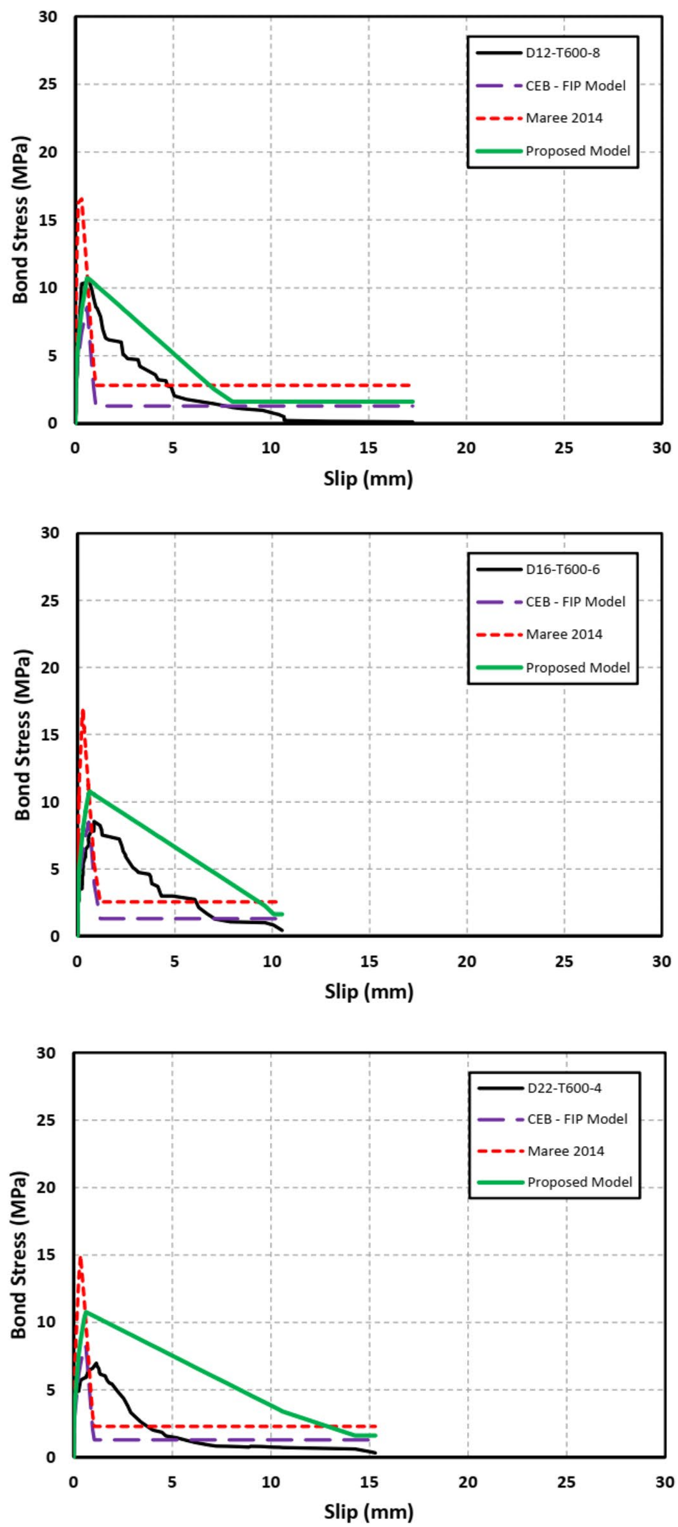

Fig. 25 Proposed analytical versus experimental bond–slip relationships (elevated temperature of 600 °C)

corresponding slippage increased due to the elevated temperatures exposure.

- Based on the obtained signal-to-noise (S/N) ratios, participation percentages and optimum levels of each considered parameters, the bond strength decreased with increasing the rebar diameter and increased slightly with increasing the L/d ratio.
- The CEB-FIP model provided more conservative values for bond strength compared to the experimental results which increase the safety level when estimating bond strength in design purposes.
- The proposed modified model achieved a higher correlation with the obtained experimental results than CEB-FIP model at ambient temperature.

Author contributions

Ismail Amer: resources, investigation, validation, visualization, writing—original draft. Mohamed Kohail: writing—review and editing, validation, conceptualization, methodology. M.S. El-Feky: writing—review and editing, validation, conceptualization, methodology. Ahmed Rashad: conceptualization, methodology, supervision. Mohamed A. Khalaf: writing—review and editing, supervision. All authors read and approved the final manuscript.

Authors information

Ismail Amer: Assistant Professor, Structural Engineering Department, Faculty of Engineering, Ain Shams University, Egypt. Mohamed Kohail: Associate Professor, Structural Engineering Department, Faculty of Engineering, Ain Shams University, Egypt. M.S. El-Feky: Associate Professor, Civil Engineering Department, National Research Centre, Egypt. Ahmed Rashad: Associate Professor, Structural Engineering Department, Faculty of Engineering, Ain Shams University, Egypt. Mohamed A. Khalaf: Professor, Structural Engineering Department, Faculty of Engineering, Ain Shams University, Egypt.

Funding

Open access funding provided by The Science, Technology & Innovation Funding Authority (STDF) in cooperation with The Egyptian Knowledge Bank (EKB).

Availability of data and materials

All data generated or analyzed during this study are included in this published article.

Declarations

Competing interests

The authors declare that they have no competing interests.

Received: 8 October 2022 Accepted: 12 March 2023
Published online: 19 June 2023

References

Abdulrahman, H., Muhamad, R., Visintin, P., & Azim Shukri, A. (2022). Mechanical properties and bond stress–slip behaviour of fly ash geopolymer concrete". *Construction and Building Materials, 327*, 126909. https://doi.org/10.1016/j.conbuildmat.2022.126909

Ahmad, M. S., & Bhargava, P. (2020). Bond slip study between concrete and steel interface using splice beam specimen exposed to elevated temperatures. *Structures, 27*, 1752–1762.

Al-Azzawi, M., Yu, T., & Hadi, M. N. S. (2018). Factors affecting the bond strength between the fly ash-based geopolymer concrete and steel reinforcement. *Structures, 14*, 262–272. https://doi.org/10.1016/j.istruc.2018.03.010

Albidah, A., Altheeb, A., Alrshoudi, F., Abadel, A., Abbas, H., & Al-Salloum, Y. (2020). Bond performance of GFRP and steel rebars embedded in metakaolin based geopolymer concrete. *Structures, 27*, 1582–1593. https://doi.org/10.1016/j.istruc.2020.07.048

Alharbi, Y. R., Abadel, A. A., Elsayed, N., Mayhoub, O., & Kohail, M. (2021a). Mechanical properties of EAFS concrete after subjected to elevated temperature. *Ain Shams Engineering Journal, 12*(2), 1305–1311. https://doi.org/10.1016/j.asej.2020.10.003

Alharbi, Y. R., Galal, M., Abadel, A. A., & Kohail, M. (2021b). Bond behavior between concrete and steel rebars for stressed elements. *Ain Shams Engineering Journal, 12*(2), 1231–1239. https://doi.org/10.1016/j.asej.2020.10.001

Allaoui, D., Nadi, M., Hattani, F., Majdoubi, H., Haddaji, Y., Mansouri, S., Oumam, M., Hannache, H., & Manoun, B. (2022). Eco-friendly geopolymer concrete based on metakaolin and ceramics sanitaryware wastes. *Ceramic International, 48*(23), 34793–34802. https://doi.org/10.1016/j.ceramint.2022.08.068

Amer, I., Kohail, M., El-Feky, M. S., Rashad, A., & Khalaf, M. A. (2020). Evaluation Of Using Cement In Alkali-Activated Slag Concrete. *International Journal of Scientific and Technology Research, 9*(05), 245–248.

Amer, I., Kohail, M., El-Feky, M. S., Rashad, A., & Khalaf, M. A. (2021a). Characterization of alkali-activated hybrid slag/cement concrete. *Ain Shams Engineering Journal, 12*(1), 135–144. https://doi.org/10.1016/j.asej.2020.08.003

Amer, I., Kohail, M., El-Feky, M. S., Rashad, A., & Khalaf, M. A. (2021b). A review on alkali-activated slag concrete. *Ain Shams Engineering Journal, 12*(2), 1475–1499. https://doi.org/10.1016/j.asej.2020.12.003

ASTM-A944. (2005). *Standard test method for comparing bond strength of steel reinforcing bars to concrete using beam-end specimens* (pp. 1–4). ASTM International.

Bamonte, P., Coronelli, D., & Gambarova, P. G. (2004). Local bond stress–slip law and size effect in high-bond bars. In *Proceedings of 5th international conference on fracture mechanics of concrete and concrete structures—FRAMCOS'5* (Vol. 2, pp. 869–876).

Bastidas, D. M., Fernández-Jiménez, A., Palomo, A., & González, J. A. (2008). A study on the passive state stability of steel embedded in activated fly ash mortars. *Corrosion Science, 50*(4), 1058–1065.

Bijen, J. (1996). Benefits of slag and fly ash. *Construction and Building Materials, 10*(5), 309–314.

Castel, A., & Foster, S. J. (2015). Bond strength between blended slag and Class F fly ash geopolymer concrete with steel reinforcement. *Cement and Concrete Research, 72*, 48–53.

Chen, H., Liu, G., Ren, J., Zhong, T., & Wang, M. (2018). Effect of high temperature on the bond performance of reinforcing bars in inorganic polymer concrete. *Journal of Advanced Concrete Technology, 16*(2), 75–83.

Comite EURO—International du Beton. (1993). *CEB-FIP model code 1990 for concrete structures*. Thomas Telford Ltd, London.

Davidovits, J. (1991). Geopolymers: Inorganic polymeric new materials. *Journal of Thermal Analysis and Calorimetry, 37*(8), 1633–1656.

Duxson, P., Provis, J. L., Lukey, G. C., & Van Deventer, J. S. J. (2007). The role of inorganic polymer technology in the development of 'green concrete.' *Cement and Concrete Research, 37*(12), 1590–1597.

Eligehausen, R., Popov, E. P., & Bertero, V. V. (1982). Local bond stress–slip relationships of deformed bars under generalized excitations.

Farghal Maree, A., & Hilal Riad, K. (2014). Analytical and experimental investigation for bond behaviour of newly developed polystyrene foam particles' lightweight concrete. *Engineering Structures, 58*, 1–11. https://doi.org/10.1016/j.engstruct.2013.10.015

Gong, C., & Yang, N. (2000). Effect of phosphate on the hydration of alkali-activated red mud–slag cementitious material. *Cement and Concrete Research, 30*(7), 1013–1016.

Grutzeck, M., Kwan, S., & DiCola, M. (2004). Zeolite formation in alkali-activated cementitious systems. *Cement and Concrete Research, 34*(6), 949–955.

Harajli, M. H., Hamad, B. S., & Rteil, A. A. (2004). Effect of confinement of bond strength between steel. *ACI Structural Journal, 101*(5), 595–603.

Jiang, X., Xiao, R., Zhang, M., Hu, W., Bai, Y., & Huang, B. (2020). A laboratory investigation of steel to fly ash-based geopolymer paste bonding behavior after exposure to elevated temperatures. *Construction and*

Building Materials, 254, 119267. https://doi.org/10.1016/j.conbuildmat.2020.119267
Khalil, M. G., Elgabbas, F., El-Feky, M. S., & El-Shafie, H. (2020). Performance of geopolymer mortar cured under ambient temperature. *Construction and Building Materials, 242*, 118090. https://doi.org/10.1016/J.CONBUILDMAT.2020.118090
Kotop, M. A., El-Feky, M. S., Alharbi, Y. R., Abadel, A. A., & Binyahya, A. S. (2021). Engineering properties of geopolymer concrete incorporating hybrid nano-materials. *Ain Shams Engineering Journal, 12*(4), 3641–3647. https://doi.org/10.1016/J.ASEJ.2021.04.022
Lee, N. K., & Lee, H.-K. (2013). Setting and mechanical properties of alkali-activated fly ash/slag concrete manufactured at room temperature. *Construction and Building Materials, 47*, 1201–1209.
Ma, C. K., Awang, A. Z., & Omar, W. (2018). Structural and material performance of geopolymer concrete: A review. *Construction and Building Materials, 186*, 90–102. https://doi.org/10.1016/j.conbuildmat.2018.07.111
Mo, K. H., Alengaram, U. J., & Jumaat, M. Z. (2016). Structural performance of reinforced geopolymer concrete members: A review. *Construction and Building Materials, 120*, 251–264. https://doi.org/10.1016/j.conbuildmat.2016.05.088
Morley, P. D., & Royles, R. (1980). The influence of high temperature on the bond in reinforced concrete. *Fire Safety Journal, 2*(4), 243–255.
Nikbakht, E., Wong Weng Lok, J., & Teo, W. (2021). Structural behaviour of novel composite beams consisting of geopolymer concrete and high-performance concrete. *Structures, 32*, 106–115. https://doi.org/10.1016/j.istruc.2021.03.014
Okoye, F. N., Durgaprasad, J., & Singh, N. B. (2015). Mechanical properties of alkali activated flyash/Kaolin based geopolymer concrete. *Construction and Building Materials, 98*, 685–691. https://doi.org/10.1016/j.conbuildmat.2015.08.009
Pal, A. (2018). Developing low-clinker ternary blends for Indian cement industry. *Journal of the Institution of Engineers (series a), 99*(3), 433–447.
Palomo, A., Grutzeck, M. W., & Blanco, M. T. (1999). Alkali-activated fly ashes: A cement for the future. *Cement and Concrete Research, 29*(8), 1323–1329.
Paswan, R., Rahman, R., Singh, S. K., & Singh, B. (2020). Bond behavior of reinforcing steel bar and geopolymer concrete. *Journal of Materials in Civil Engineering, 32*(7), 4020167. https://doi.org/10.1061/(ASCE)MT.1943-5533.0003237
Provis, J. L., & Van Deventer, J. S. J. (2009). Introduction to geopolymers. In *Geopolymers* (pp. 1–11). Elsevier.
Provis, J. L., & Van Deventer, J. S. J. (2009). *Geopolymers: structures, processing, properties and industrial applications*. Elsevier.
Puertas, F., Martinez-Ramirez, S., Alonso, S., & Vazquez, T. (2000). Alkali-activated fly ash/slag cements: strength behaviour and hydration products. *Cement and Concrete Research, 30*(10), 1625–1632.
Ramagiri, K. K., & De Maeijer, P. K. (2022). High-temperature, bond, and environmental impact assessment of alkali-activated concrete (AAC). *Infrastructures, 7*(9), 119. https://doi.org/10.3390/infrastructures7090119
Ravikumar, D., Peethamparan, S., & Neithalath, N. (2010). Structure and strength of NaOH activated concretes containing fly ash or GGBFS as the sole binder. *Cement and Concrete Composites, 32*(6), 399–410.
Refaat, M., Mohsen, A., Nasr, E.-S.A.R., & Kohail, M. (2021). Minimizing energy consumption to produce safe one-part alkali-activated materials. *Journal of Cleaner Production, 323*, 129137. https://doi.org/10.1016/j.jclepro.2021.129137
Romanazzi, V., Leone, M., Aiello, M. A., & Pecce, M. R. (2022). Bond behavior of geopolymer concrete with steel and GFRP bars. *Composite Structures, 300*, 116150. https://doi.org/10.1016/j.compstruct.2022.116150
Sarker, P. K. (2011). Bond strength of reinforcing steel embedded in fly ash-based geopolymer concrete. *Materials and Structures, 44*(5), 1021–1030.
Shamseldein, A., Elshafie, H., Rashad, A., & Kohail, M. (2018). Assessment and restoration of bond strength of heat-damaged reinforced concrete elements. *Construction and Building Materials, 169*, 425–435.
Sofi, M., Van Deventer, J. S. J., Mendis, P. A., & Lukey, G. C. (2007). Bond performance of reinforcing bars in inorganic polymer concrete (IPC). *Journal of Materials Science, 42*(9), 3107–3116.
Thomas, R. J., & Peethamparan, S. (2015). Alkali-activated concrete: Engineering properties and stress–strain behavior. *Construction and Building Materials, 93*, 49–56.
Unis Ahmed, H., Mahmood, L. J., Muhammad, M. A., Faraj, R. H., Qaidi, S. M. A., Sor, N. H., Mohammed, A. S., & Mohammed, A. A. (2022). Geopolymer concrete as a cleaner construction material: An overview on materials and structural performances. *Cleaner Materials, 5*, 100111. https://doi.org/10.1016/j.clema.2022.100111
Wu, Y.-F., & Zhao, X.-M. (2013). Unified bond stress–slip model for reinforced concrete. *Journal of the Structural Engineering. American Society of Civil Engineers, 139*(11), 1951–1962.
Xie, J., Wang, J., Rao, R., Wang, C., & Fang, C. (2018). Effects of combined usage of GGBS and fly ash on workability and mechanical properties of alkali activated geopolymer concrete with recycled aggregate. *Composites Part b: Engineering, 164*, 179–190. https://doi.org/10.1016/j.compositesb.2018.11.067
Xu, Y. (1990). Experimental study of anchorage properties for deformed bars in concrete. Beijing, Tsinghua.
Yang, T., Shenchun, X., Liu, Z., Li, J., Pengtao, W., Yang, Y., & Chengqing, W. (2022). Experimental and numerical investigation of bond behavior between geopolymer based ultra-high-performance concrete and steel bars. *Construction and Building Materials, 345*, 128220. https://doi.org/10.1016/j.conbuildmat.2022.128220
Yin, K. F., Han, Y., & Liu, Y. (2011). Experimental research on bond strength between rebar and concrete after high temperature. *Applied Mechanics and Materials, 71*, 1057–1061.
Zhang, H. Y., Kodur, V., Wu, B., Yan, J., & Yuan, Z. S. (2018). Effect of temperature on bond characteristics of geopolymer concrete. *Construction and Building Materials, 163*, 277–285.
Zhang, H., Yan, J., & Wu, B. (2016). Study on bond behavior between geopolymer concrete and steel bars. *China Civil Engineering Journal, 49*(7), 107–115.
Zhang, P., Wang, K., Li, Q., Wang, J., & Ling, Y. (2020). Fabrication and engineering properties of concretes based on geopolymers/alkali-activated binders—A review. *Journal of Cleaner Production, 258*, 120896.

Publisher's Note

Dr. Ismail Amer Assistant Professor of Structural Engineering at Ain Shams University, Cairo, Egypt. He obtained his M.Sc., Structural Engineering, in 2017, from Ain Shams University on the strengthening of steel beams using advanced composite materials, FRP. He completed his Ph.D., Structural Engineering, in 2021, from Ain Shams University on the characterization and development of alkali-activated concrete to be introduced in the construction field as a step towards sustainability. His major area of research includes repair and strengthening of structures, new concrete technologies, and innovative and sustainable construction materials such as Geopolymer Concrete, Alkali Activated Concrete and Reactive Powder Concrete. He has published several papers in leading international journals. He is also a certified reviewer in several highly regarded scientific journals affiliated with international publishers such as ASCE, ScienceDirect and Wiley. He has over 13 years of experience in teaching, research, and consultancy in the field of structural Engineering.

Dr. Mohamed Kohail Associate Professor at Ain Shams University's Faculty of Engineering in the Structural Engineering Department. He specializes in the areas of innovative and eco-friendly building materials, sustainability, and energy in buildings. With extensive research expertise, he has authored several highly regarded publications in leading academic journals. Dr. Kohail has worked with various international research groups across multiple disciplines, providing valuable insights to tackle pressing global challenges. His contributions to the field of sustainable construction and engineering have garnered widespread recognition, establishing him as a prominent thought leader in his area of expertise.

Dr. M. S. El-Feky is a researcher at the national research centre of Egypt, received his Ph.D. in 2014 on the effect of nano materials on concrete properties, and since then he worked on the field of nano construction materials, and advanced geopolymer concretes with the concern of the environmental and financial aspects.

Dr. Ahmed Rashad was graduated from Structural Engineering department, Faculty of Engineering, Ain Shams University, Cairo, Egypt in 1996. He got his M.Sc. from the same department in 2001 in the field of CORROSION OF STEEL REINFORCEMENT. He got his Ph.D. from the same department in 2008 in the field of BEHAVIOR OF MASONERY STRUCTURES. He was Assoc. Professor of properties and testing of materials in the same department. His major scientific research interest is in the fields of corrosion of steel reinforcement, repair and strengthening of RC and masonry structures, applications of FRP materials in the structural field, and geopolymer concrete

Prof. Dr. Mohamed A. Khalaf was graduated from Structural Engineering Department, Faculty of Engineering, Ain Shams University, Cairo, Egypt in June1990. He got his M.Sc. from the same department in 1993 in the field of CATHODIC PROTECTION OF STEEL REINFORCEMENT. He got his Ph.D. from Drexel University, PA, USA in 2001 in the field of FATIGUE BEHAVIOR OF GFRP PULTRUDED BEAMS. Now he is a professor of properties and strength of materials in the same department. His scientific research interest is in the fields of corrosion of steel reinforcement, repair and strengthening of RC structures, applications of FRP materials in the structural field, and properties and applications of geopolymer concrete.